Nonlinear Moment-Based Optimal Control of Wave Energy Converters With Non-Ideal Power Take-Off Systems

Proceedings of Proceedings of the ASME 2022 41st International Conference on Ocean, Offshore and Arctic Engineering OMAE2022
June 5-10, 2022, Hamburg, Germany

OMAE2022-81267

NONLINEAR MOMENT-BASED OPTIMAL CONTROL OF WAVE ENERGY CONVERTERS WITH NON-IDEAL POWER TAKE-OFF SYSTEMS

Nicolás Faedo
Marine Offshore Renewable Energy Lab.
Department of Mechanical and Aerospace Engineering
Politecnico di Torino
Torino, Italy
Email: nicolas.faedo@polito.it

Giuseppe Giorgi
Marine Offshore Renewable Energy Lab.
Department of Mechanical and Aerospace Engineering
Politecnico di Torino
Torino, Italy
Email: giuseppe.giorgi@polito.it

Giuliana Mattiazzo
Marine Offshore Renewable Energy Lab.
Department of Mechanical and Aerospace Engineering
Politecnico di Torino
Torino, Italy
Email: giuliana.mattiazzo@polito.it

John V. Ringwood
Centre for Ocean Energy Research
Department of Electronic Engineering
Maynooth University
Kildare, Ireland
Email: john.ringwood@mu.ie

ABSTRACT

The mechanical-to-electrical energy conversion stage in wave energy devices is commonly affected by losses associated with the power take-off (PTO) system, inevitably leading to non-ideal conversion in practical scenarios. Such behaviour needs to be incorporated within the wave energy converter (WEC) energy-maximising control design procedure, so as to guarantee optimal operation of the device under these non-ideal conditions. Motivated by this requirement, we present, in this paper, a nonlinear moment-based energy-maximising control solution for WECs under non-ideal PTO behaviour. We show that the mathematical formalism proposed always admits a globally optimal energy-maximising solution, facilitating the application of state-of-the-art numerical routines, leading to real-time performance. Numerical results are presented for a heaving point absorber WEC system, illustrating the capabilities of the proposed controller in a non-ideal PTO conversion scenario, including a comparison with a benchmark control strategy.

1 Introduction

The path towards successful commercialisation of wave energy technology inherently encompasses the design and synthesis of appropriate *energy-maximising* control technology, capable of achieving maximum energy extraction from the incoming wave field [1, 2], hence having the potential of substantially reducing the associated levelised cost of wave energy.

Though the last decade saw significant growth in tailored optimal control strategies for wave energy converters (WEC) (see *e.g.* the review papers [3, 4]), the vast majority of WEC controllers attempt to maximise hydrodynamic energy absorption, *i.e.* inherently assuming that the mechanical-to-electrical energy conversion stage at the power take-off (PTO) system is *ideal*. Although such idealised conditions can simplify the control design and synthesis procedure, often leading to powerful, yet tractable, energy-maximising control algorithms, the assumption of 'perfect' power conversion can be somewhat limiting in practical applications. In particular, a truly optimal control regime vir-

tually always requires[1], by definition, *reactive* power flux (*i.e.* injection of power from the grid to the WEC system) to achieve maximum mechanical energy extraction from the incoming wave field. During this reactive power phase, the PTO actuator (generator) is effectively behaving as a motor, and can suffer a significant drop in its operating efficiency. Such a non-ideal behaviour can have a severe impact in energy absorption performance, especially if the optimal controller does not incorporate such information at the design stage (see *e.g.* [7–9]).

A particularly efficient direct optimal control framework for WEC systems was recently introduced in [10–13], built upon so-called moment-based theory [14, 15]. *Moments* are mathematical objects which, under certain assumptions, can provide a convenient parameterisation of the steady-state behaviour of the WEC system for a given class of inputs, including those typically characterising the WEC energy harvesting process. Such a parameterisation can be explicitly used to transcribe the associated WEC control problem into a well-posed finite-dimensional nonlinear program, which always admits a global energy maximising solution, and can hence be effectively computed in real-time (*i.e.* is tractable). Though convenient for the numerical solution of a nonlinear WEC control problem, the moment-based framework presented in [10–13] considers a unitary mechanical-to-electrical conversion stage, *i.e.* an idealised PTO system, which can be limiting when realistic conversion mechanisms are involved.

Motivated by this, we present, in this paper, an extension of the nonlinear moment-based framework in [10], which incorporates non-ideal PTO behaviour. In particular, we consider that the mechanical-to-electrical conversion depends upon a discontinuous efficiency map, influencing the absorption dynamics for both reactive, and passive power flow cases. Throughout our manuscript, we demonstrate that the attractive properties of moment-based control for ideal PTO systems are effectively retained in this non-ideal PTO counterpart, including well-posedness (*i.e.* existence of globally optimal solutions) of the corresponding nonlinear program, and real-time capabilities. Furthermore, we illustrate the performance of the proposed control solution in terms of a case study, involving a heaving point absorber WEC system inspired by [16].

The remainder of this paper is organised as follows. Section 1.1 presents the main notation used throughout our study, while Section 2 presents the dynamics associated with the considered WEC system. Section 3 introduces the definition of the receding-horizon WEC optimal control problem under non-ideal PTO energy conversion, while Section 4 presents the proposed moment-based control solution. Finally, Section 5 discusses the performance of the optimal controller for the selected WEC system, while Section 6 encompasses the conclusions of our study.

[1]As a matter of fact, the only case where reactive power is not required to achieve optimality takes place when the input wave is monochromatic, and has the exact same frequency as that characterising the resonance frequency of the corresponding WEC system (see *e.g.* [5, 6]).

1.1 Notation and conventions

$\mathbb{R}^+$ ($\mathbb{R}^-$) denotes the set of non-negative (non-positive) real numbers. $\mathbb{C}^0$ denotes the set of pure-imaginary complex numbers. The symbol 0 stands for any zero element, dimensioned according to the context. The symbol $\mathbb{I}_n$ denotes the identity matrix in $\mathbb{C}^{n\times n}$. The superscript $\intercal$ denotes the transposition operator. The spectrum of a matrix $A \in \mathbb{R}^{n\times n}$, *i.e.* the set of its eigenvalues, is denoted by $\lambda(A)$. The *Kronecker product* between two matrices M_1 and M_2 is denoted by $M_1 \otimes M_2$. The *vectorization* operator acting on a matrix $A \in \mathbb{C}^{n\times m}$ is denoted as $\mathrm{vec}(A) \in \mathbb{C}^{nm}$. Finally, given two functions f_1 and f_2, such that $f_1 : \mathscr{X} \to \mathscr{Y}$ and $f_2 : \mathscr{Z} \to \mathscr{X}$, the composition $f_1(f_2(z))$, which maps all $z \in \mathscr{Z}$ to $f_1(f_2(z)) \in \mathscr{Y}$, is denoted as $f_1 \circ f_2$.

2 Point absorber dynamics

Throughout our manuscript, we consider a heaving point absorber WEC device, inspired by the design presented in *e.g.* [16]. The system, which is schematically illustrated in Figure 1 (along with its corresponding dimensions in metres), is essentially an offshore WEC, where energy from incoming waves is extracted from the heave (translational) mode of motion.

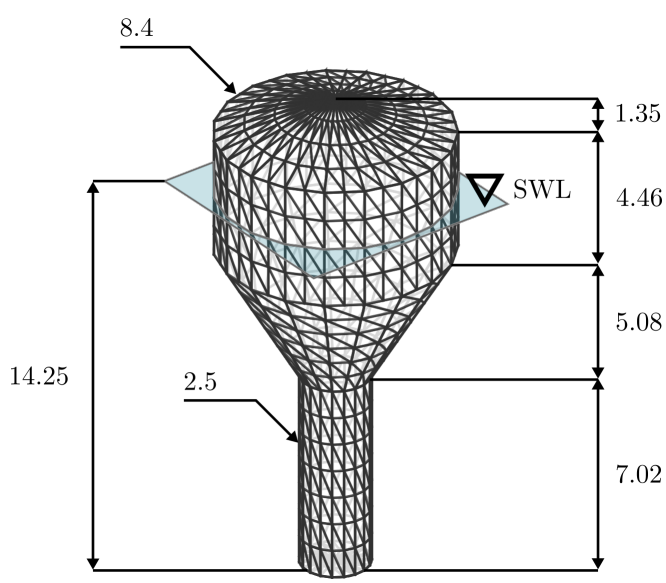

FIGURE 1. Point absorber device under study (dimensions in [m]).

If we constrain the WEC to move in a single degree-of-freedom[2] (DoF), *i.e.* heave, the equation of motion of such a device can be expressed as a finite-dimensional dynamical system Σ, characterised in terms of an associated differential equation,

[2]We consider a single-DoF system for simplicity of notation. Similar modelling considerations can be made for a multi-DoF WEC system (see, *e.g.* [2]).

given (see [10, 17]) by[3]

$$\Sigma : \begin{cases} \ddot{z} = \mathscr{M}\left(f_{rad} + f_e + f_v + f_{re} - u\right), \\ y = \dot{z}, \end{cases} \tag{1}$$

where $z : \mathbb{R}^+ \to \mathbb{R}$ denotes the displacement of the device, $f_{rad} : \mathbb{R}^+ \to \mathbb{R}$ the radiation force (which accounts for the fluid memory effects), $f_v : \mathbb{R}^+ \to \mathbb{R}$ the viscous force, f_{re} the restoring force, $f_e : \mathbb{R}^+ \to \mathbb{R}$, the wave excitation force (*i.e.* external uncontrollable input representing the force exerted by waves on the surface of the device), $u : \mathbb{R}^+ \to \mathbb{R}$, the control input (to be optimally designed), and $\mathscr{M} \in \mathbb{R}_{>0}$ is the inverse of the generalised WEC mass (see *e.g.* [18]).

The radiation force is characterised by a linear, continuous-time, strictly proper, passive, finite-dimensional[4] system Σ_r, which directly depends upon the output of system (1). Without any loss of generality, such an output feedback system can be expressed, in state-space, as

$$\Sigma_r : \begin{cases} \dot{\Gamma} = F\Gamma + G\dot{z}, \\ f_{rad} = H\Gamma, \end{cases} \tag{2}$$

with $\Gamma(t) \in \mathbb{R}^{n_r}$, $F \in \mathbb{R}^{n_r \times n_r}$, and $\{G, H^\intercal\} \subset \mathbb{R}^{n_r}$. The mapping f_v, characterising viscous effects, is written in terms of a smooth approximation of the so-called Morison equation [21], *i.e.*

$$f_v = -\alpha_v \dot{z}\sqrt{\dot{z}^2 + \varepsilon}, \tag{3}$$

with $\varepsilon \in \mathbb{R}^+$ sufficiently small, and $\alpha_v \in \mathbb{R}^+$ directly depending on the physical dimensions of the device. The restoring force f_r is expressed in terms of a polynomial map in z (see [10, 16]), *i.e.*

$$f_{re} = -\beta_{r_0} z + \beta_{r_1} z^2 + \beta_{r_2} z^3, \tag{4}$$

where $\beta_{r_0} \in \mathbb{R}^+$ is commonly referred to as hydrostatic stiffness, and $\{\beta_{r_1}, \beta_{r_2}\} \subset \mathbb{R}$.

With the specific definitions for the mappings offered above, system Σ in (1) can be expressed in state-space form as

$$\Sigma : \begin{cases} \dot{x} = f(x, \zeta) = Ax + B\zeta + g(x), \\ y = h(x) = Cx, \end{cases} \tag{5}$$

with $\zeta = f_e - u$ the total input force, and where the associated state vector is defined as $x = [z\ \dot{z}\ \Gamma^\intercal]^\intercal$, $x(t) \in \mathbb{R}^n$, with $n = 2 + n_r$.

The triple of matrices (A, B, C), with $A \in \mathbb{R}^{n \times n}$, $\{B, C^\intercal\} \subset \mathbb{R}^n$, is given by

$$A = \begin{bmatrix} A^0 & -B^0 H \\ GC^0 & F \end{bmatrix},\ B = \begin{bmatrix} B^0 \\ 0 \end{bmatrix},\ C = \begin{bmatrix} C^0 & 0 \end{bmatrix}, \tag{6}$$

together with

$$A^0 = \begin{bmatrix} 0 & 1 \\ -\mathscr{M}\beta_{r_0} & 0 \end{bmatrix},\ B^0 = \begin{bmatrix} 0 \\ \mathscr{M} \end{bmatrix},\ C^0 = \begin{bmatrix} 0 & 1 \end{bmatrix}. \tag{7}$$

The mapping $g : \mathbb{R}^n \to \mathbb{R}^n$, which is exclusively composed of terms characterising the nonlinear behaviour of system (1), can be written as

$$g(x) = \begin{bmatrix} g^0(x) \\ 0 \end{bmatrix}, \tag{8}$$

with g^0 defined as

$$g^0(x) = \begin{bmatrix} 0 \\ -\alpha_v x_2 \sqrt{\dot{x}_2{}^2 + \varepsilon} + \beta_{r_1} x_1^2 + \beta_{r_2} x_1^3 \end{bmatrix}. \tag{9}$$

Note that the smooth mappings g and g^0 are such that $g(0) = 0$ and $g^0(0) = 0$ so that, clearly, $f(0,0) = 0$ and $h(0) = 0$, and $(0,0)$ is an equilibrium (invariant) point of $\dot{x} = f(x, 0)$.

3 Optimal control problem: Preliminaries

WEC energy-maximising control design procedures can be defined in terms of an associated optimal control problem[5] (OCP), characterised in terms of a corresponding objective function $\mathscr{J}$. Throughout the reminder of this paper, we adopt a *receding-horizon* approach (see *e.g.* [23]) for the definition of such an associated OCP. In particular, let $T \in \mathbb{R}^+$ be the *time-horizon*, where one effectively optimises energy capture within an associated *time-window* $\Xi_N = [N\Delta_h, N\Delta_h + T] \subset \mathbb{R}^+$, $N \in \mathbb{N}$, by means of an optimal control input $u_N^{\text{opt}} : \Xi_N \to \mathbb{R}$, and where $\Delta_h \in \mathbb{R}^+$ denotes the *receding time-step*.

For each window Ξ_N, the ultimate aim is to maximise the energy absorbed from the incoming wave field, which can be explicitly written in terms of an objective map $u \mapsto \mathscr{J}(u)$, such that

$$\mathscr{J}(u) = \frac{1}{T}\int_{\Xi_N} u(\tau)y(\tau)d\tau = \frac{1}{T}\int_{\Xi_N} p_{\text{m}}(\tau)d\tau, \tag{10}$$

[3] From now on, the dependence on t is dropped when clear from the context.

[4] See [19, 20] for a formal discussion on the properties associated with Σ_r.

[5] The reader is referred to [22] for a formal treatment of optimal control theory.

where y is defined as in (5), and $p_{\mathrm{m}} = uy$ denotes the hydrodynamic (*i.e.* mechanical) instantaneous power. With the definition of the control objective map (10), the receding-horizon WEC OCP can be formalised in terms of the following problem (P_{m}):

$$
\begin{aligned}
(P_{\mathrm{m}}): \quad & u_N^{\mathrm{opt}} = \arg\max_{u_N} \frac{1}{T}\int_{\Xi_N} u(\tau)y(\tau)d\tau, \\
& \text{subject to} \\
& \dot{x} = Ax + B\zeta + g(x), \\
& y = Cx, \\
& (x, u_N) \in \mathscr{X} \times \mathscr{U}, \forall t \in \Xi_N,
\end{aligned} \tag{11}
$$

where $\mathscr{X} \subset \mathbb{R}^n$ and $\mathscr{U} \subset \mathbb{R}$, with $\mathscr{X}$ closed, $\mathscr{U}$ compact, and where $(0,0) \in \mathscr{X} \times \mathscr{U}$, define the so-called state and input constraints, respectively.

3.1 Non-ideal PTO conversion behaviour

The OCP defined in (11) is built upon the premise of maximising hydrodynamic power absorption, *i.e.* raw mechanical power from the incoming wave field. This is consistent with an ideal PTO conversion system, where the mechanical-to-electrical energy map is effectively unity, *i.e.* $p_{\mathrm{m}} = p_{\mathrm{e}}$, with p_{e} denoting the electric power. As discussed throughout Section 1, in practical scenarios, such an assumption can be limiting, since the PTO system is virtually always non-ideal: The electrical power p_{e}, seen from the PTO side, is effectively different from the (ideal) hydrodynamic power p_{m}, due to the losses occurring throughout the conversion stage. This behaviour is often modelled in terms of a associated efficiency map $\eta : \mathbb{R} \to \mathbb{R}$, $p_{\mathrm{m}} \mapsto \eta(p_{\mathrm{m}})$, describing the mechanical-to-electric conversion stage $p_{\mathrm{m}} \mapsto p_{\mathrm{e}}$ (see *e.g.* [7, 24]). In particular, when the optimal control procedure (11) necessitates *reactive* power flow, *i.e.* the power flows from the grid to the device ($p_{\mathrm{m}} < 0$), and hence the actuator is effectively operating as a motor, it virtually always requires more electrical power supply than the mechanical power it can actually deliver to the WEC system. On the contrary, if $p_{\mathrm{m}} > 0$ (*passive* power flow), the power at the end of the PTO system tends to be smaller than the mechanical power absorbed from the incoming wave field by the WEC device.

To (formally) incorporate such a non-ideal PTO behaviour in the control design procedure, we consider the following efficiency map, which has been considered explicitly within the control benchmark case set by the Wave Energy Control Competition (WECCCOMP) (see *e.g.* [25, 26]):

$$
\eta(p_{\mathrm{m}}) = \frac{\mu^2 - 1}{2\mu}\mathrm{sign}(p_{\mathrm{m}}) + \frac{\mu^2 + 1}{2\mu}, \tag{12}
$$

where $\mu \in [0, 1]$ is the so-called *efficiency factor* (which corresponds to the product of the average efficiencies of each potential PTO conversion stage). Note that the corresponding electrical power is hence straightforwardly defined by

$$
p_{\mathrm{e}}(p_{\mathrm{m}}) = \eta(p_{\mathrm{m}})p_{\mathrm{m}} = \begin{cases} \mu p_{\mathrm{m}} & \text{if } p_{\mathrm{m}} > 0, \\ 0 & \text{if } p_{\mathrm{m}} = 0, \\ \dfrac{p_{\mathrm{m}}}{\mu} & \text{if } p_{\mathrm{m}} < 0. \end{cases} \tag{13}
$$

With the definition of p_{e} in (13), the associated WEC OCP can be directly written in terms of problem (P_{m}), with the incorporation of the corresponding efficiency map η. To be precise, such a scenario can be defined in terms of the following maximisation problem (P_{e}) for electrical energy absorption:

$$
\begin{aligned}
(P_{\mathrm{e}}): \quad & u_N^{\mathrm{opt}} = \arg\max_{u_N} \frac{1}{T}\int_{\Xi_N} \eta(u(\tau)y(\tau))u(\tau)y(\tau)d\tau, \\
& \text{subject to} \\
& \dot{x} = Ax + B\zeta + g(x), \\
& y = Cx, \\
& (x, u_N) \in \mathscr{X} \times \mathscr{U}, \forall t \in \Xi_N.
\end{aligned} \tag{14}
$$

4 Direct optimal control via moment-based theory

Either in the case of problem (P_{m}) or (P_{e}), the WEC energy-maximising OCP is defined over an infinite-dimensional function space. As such, a common practice for this type of OCPs, is that of *direct transcription* (see *e.g.* [27]), *i.e.* suitable discretisation of the associated state and input variables, so that the infinite-dimensional OCP can be *transcribed* into a (finite-dimensional) nonlinear program (NP). If the transcription is adequate (*i.e.* well-posed), the resulting NP can be subsequently solved via state-of-the-art numerical routines, facilitating real-time solution of either (P_{m}) or (P_{e}).

A particularly efficient direct optimal control solution, to solve for the ideal WEC OCP (P_{m}), has been recently introduced in [10–13], built upon so-called moment-based theory [14, 15]. *Moments* are mathematical objects which, under certain assumptions, can provide a convenient parameterisation of the steady-state behaviour of the WEC system (5) for a given class of inputs, including those characterising the WEC energy harvesting process. Such a parameterisation can be explicitly used to transcribe the associated OCP into a well-posed NP, *i.e.* a finite-dimensional nonlinear program which always admits a global energy maximising solution and can be effectively computed in real-time.

We show, throughout this section, that the nonlinear moment-based framework in [10] can be effectively extended to WEC systems incorporating non-ideal PTO behaviour, *i.e.* to

solve problem (P_{e}) in (14). In particular, we show that the resulting NP is also well-posed, and can hence inherently retain the benefits of the strategy when applied to the ideal OCP (P_{m}).

4.1 Moment-based representation

We (very briefly) recall the fundamentals behind moment-based theory for WEC systems, as developed in *e.g.* [10–13]. In particular, within moment-based optimal control, both the external (uncontrollable) wave excitation force, and the corresponding control input, are defined in terms of an implicit-form description. In particular, for each time-window Ξ_N, both maps f_e and u_N are written in terms of an appropriate finite-dimensional set of first-order differential equations[6], termed a *signal generator* (or exogenous system [28]) $\mathscr{G}_N$, *i.e.*

$$\mathscr{G}_N : \begin{cases} \dot{\xi} = S\xi, \\ f_e = \overline{L_e}\xi, \\ u_N = \overline{L_u}\xi, \end{cases} \tag{15}$$

with $S \in \mathbb{R}^{\nu\times\nu}$, $\nu \in 2\mathbb{Z}/0$, such that $\lambda(S) = \{\mathrm{i}k\omega_0\}_{k=1}^{\nu/2} \subset \mathbb{C}^0$, and where the triple of matrices $(S, \xi(N\Delta_h), \overline{L_e} - \overline{L_u})$ is assumed to be minimal $\forall N \in \mathbb{N}$. Given the nature of the state-transition mapping f in (5), there exists [10, 14] a unique mapping π such that, for any fixed trajectory $\xi(t)$ of $\mathscr{G}_N$, the steady-state response x_{ss} of system Σ in (5), driven by $\mathscr{G}_N$, is $x_{\mathrm{ss}}(t) = \pi(\xi(t))$. We term the composition mapping $\mathscr{M} = h \circ \pi$ the *moment* of system Σ at $\mathscr{G}_N$. Note that, under this definition, the computation of the moment at a particular trajectory $\xi(t)$ of the signal generator (15) coincides with the steady-state output response of Σ driven by $\mathscr{G}_N$, *i.e.* $y_{\mathrm{ss}}(t) = h(x_{\mathrm{ss}}(t)) = h(\pi(\xi(t)))$.

Following [10, 29], an approximation of the moment $\mathscr{M}$ can be computed, for any ν sufficiently large, in terms of a finite-dimensional expansion over the set spanned by $\{\xi_i\}_{i=1}^{\nu/2}$, *i.e.* $\mathscr{M}(\xi) \approx \bar{Y}\xi$, with $\bar{Y}^{\intercal} \in \mathbb{R}^{\nu}$, and hence, for a given trajectory $\xi(t)$, $y_{\mathrm{ss}}(t) \approx \bar{Y}\xi(t)$. In particular, [10, 29] follows a Galerkin-like approach (see also [30]) for the computation of $\bar{Y}^{\intercal}$, by using the following definitions[7]:

$$\begin{aligned} \Omega &= \left[\xi(t_1^N) \ \dots \ \xi(t_w^N)\right], \\ G(\bar{Y}) &= \left[g(\bar{Y}\xi(t_1^N)) \ \dots \ g(\bar{Y}\xi(t_w^N))\right], \\ \bar{\Phi} &= (\mathbb{I}_\nu \otimes C)\Phi^{-1}(\mathbb{I}_\nu \otimes -B), \\ \Phi_\Omega &= (\mathbb{I}_\nu \otimes C)\Phi^{-1}(\Omega^{-1^{\intercal}} \otimes \mathbb{I}_n), \\ \Phi &= (S \otimes \mathbb{I}_n) + (\mathbb{I}_\nu \otimes A), \end{aligned} \tag{16}$$

with $\mathscr{T}_N = \{t_1^N, \dots, t_w^N\} \subset \Xi_N$ a set of w uniformly-spaced collocation instants, with w sufficiently large.

Via the definitions recalled in (16), $\bar{Y}$ can be computed as the unique solution of the following nonlinear algebraic matrix equation

$$\bar{Y} - (\overline{L_e} - \overline{L_u})\bar{\Phi}^{\intercal} + \mathrm{vec}(G(\bar{Y}))^{\intercal}\bar{\Phi}_\Omega^{\intercal} = 0. \tag{17}$$

In other words, the adopted moment-based framework facilitates a finite-dimensional parameterisation of y_{ss} in terms of $\bar{Y}$, the solution of (17), which can be explicitly used to transcribe the OCP (P_{e}), as demonstrated in Section 4.3.

4.2 Smooth approximation of η

Before describing the moment-based transcription process associated with problem (P_{e}), we note that the mapping η in (12), defining the PTO conversion efficiency, is of a discontinuous nature. This, naturally, has an impact on the definition of the associated OCP (P_{e}), which is consequently inherently discontinuous. The non-differentiability of the control objective at $p_{\mathrm{m}} = 0$ can potentially lead to numerical issues when solving the resulting NP via standard numerical routines, which generally attempt to compute an approximation of the first- and/or second-order derivatives of the corresponding objective at each iteration. To circumvent this issue, we propose the use of a C^∞ approximation of η within the optimal control design and computation procedure, defined in terms of a *sigmoid* function, *i.e.*

$$\eta(p_{\mathrm{m}}) \approx \tilde{\eta}(p_{\mathrm{m}}) = \frac{\mu^2 - 1}{\mu}\mathrm{sigm}(p_{\mathrm{m}}, l) + \frac{1}{\mu}, \tag{18}$$

where $\mathrm{sigm} : \mathbb{R} \times \mathbb{R}^+ \to \mathbb{R}$ is defined as

$$\mathrm{sigm}(p_{\mathrm{m}}, l) = \frac{1}{1 + e^{-l p_{\mathrm{m}}}}. \tag{19}$$

The value l in (19) can be used to adjust the rate of change of the function about the inflexion point $p_{\mathrm{m}} = 0$, *i.e.* it defines the quality of the approximation when p_{m} approaches the non-differentiable centre point of the efficiency map η. Figure 2 provides a graphical illustration of the approximation offered by $\tilde{\eta}$.

4.3 Direct transcription of (P_{e})

The moment-based parameterisation of the steady-state response of the WEC system, discussed in Section 4.3, *i.e.* $y_{\mathrm{ss}} = \bar{Y}\xi$, with $\bar{Y}$ the solution of equation (17), can be explicitly used to transcribe the non-ideal WEC OCP (P_{e}) into a well-posed NP. In

[6] We note that the suitability of the implicit form representation (15), for any N, has been demonstrated and discussed in [13].

[7] The reader is referred to [10] for the explicit derivation of each term presented in equation (16).

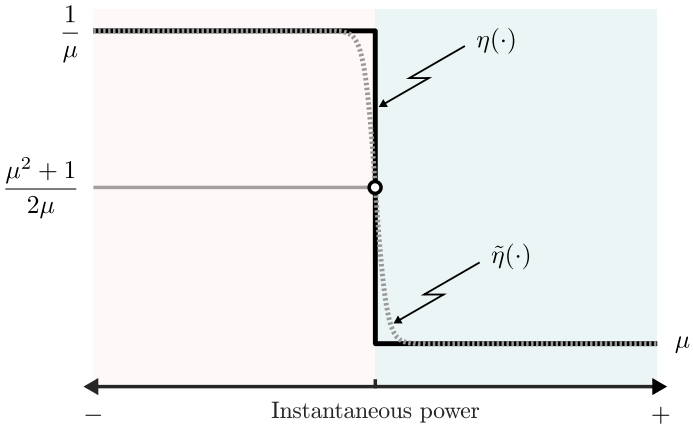

FIGURE 2. Smooth approximation $\tilde{\eta}$ of the efficiency map η.

particular, the solution u_N^{opt} of problem (P_{e}) can be approximated by that of the finite-dimensional NP $\widetilde{(P_{\text{e}})}$, defined over $\mathbb{R}^{\nu}$, as

$$\begin{aligned}\widetilde{(P_{\text{e}})}:\ \overline{L_u^{\text{opt}}} &= \arg\max_{\overline{L_u}^{\intercal}\in\mathbb{R}^{\nu}} \frac{1}{T}\int_{\Xi_N} \tilde{\eta}(\overline{L_u}\xi(t)\bar{Y}\xi(t))\overline{L_u}\xi(t)\bar{Y}\xi(t)d\tau,\\ &\text{subject to}\\ &\bar{Y}-(\overline{L_e}-\overline{L_u})\bar{\Phi}^{\intercal}+\text{vec}(G(\bar{Y}))^{\intercal}\bar{\Phi}_{\Omega}^{\intercal}=0,\\ &(\bar{Y}\xi,\overline{L_u}\xi)\in\mathscr{X}\times\mathscr{U},\forall t\in\mathscr{T}_N.\end{aligned} \tag{20}$$

where the corresponding optimal control input is computed from (20) as $u_N^{\text{opt}}=\overline{L_u^{\text{opt}}}\xi$. Note that the corresponding state and input constraints are now 'enforced' at the finite-set $\mathscr{T}_N\subset\Xi_N$.

We now show two fundamental properties underlying the NP defined by problem $\widetilde{(P_{\text{e}})}$: (1) the moment-based equality constraint in $\widetilde{(P_{\text{e}})}$ can be explicitly included as part of the objective function (hence alleviating the computational expense behind solving the corresponding NP), and (2) problem $\widetilde{(P_{\text{e}})}$ is well-posed, *i.e.* it always admits a globally optimal energy maximising solution, even in the presence of the non-ideal PTO efficiency map η. To derive these properties, let us define $\mathscr{I}\in\mathbb{R}$ as $\mathscr{I}=\int_{\Xi_N}\tilde{\eta}(\overline{L_u}\xi\bar{Y}\xi)\overline{L_u}\xi\bar{Y}\xi d\tau$, for any admissible pair $(\bar{Y},\overline{L_u})$. We begin by noting that the following identity for $\mathscr{I}$ follows trivially

$$\begin{aligned}\mathscr{I}&=\mathscr{I}_{\text{m}}+\mathscr{I}_{\text{e}},\\ \mathscr{I}_{\text{m}}&=\int_{\Xi_N}\overline{L_u}\xi(t)\bar{Y}\xi(t)d\tau,\\ \mathscr{I}_{\text{e}}&=\int_{\Xi_N}(\tilde{\eta}(\overline{L_u}\xi(t)\bar{Y}\xi(t))-1)\overline{L_u}\xi(t)\bar{Y}\xi(t)d\tau,\end{aligned} \tag{21}$$

where $\mathscr{I}_m$ corresponds to 'pure' (ideal) mechanical average power extraction, while $\mathscr{I}_e$ reflects the effect of the non-ideal electrical conversion stage. Given the nature of the spectrum associated with the signal generator defined in (15), the term $\mathscr{I}_m$ can be further evaluated (see [10]) as

$$\mathscr{I}_{\text{m}}=\bar{Y}\left(\int_{\Xi_N}\xi(t)\xi(t)^{\intercal}d\tau\right)\overline{L_u}^{\intercal}=\frac{T}{2}\bar{Y}\overline{L_u}^{\intercal}. \tag{22}$$

Since $0\notin\lambda(\bar{\Phi})$ (see [10]), we further note that, for any admissible $\bar{Y}$, the vector $\bar{L}_u$ can be uniquely written in terms of the former, *i.e.*

$$\overline{L_u}=-(\bar{Y}+\text{vec}(G(\bar{Y}))^{\intercal}\bar{\Phi}_{\Omega}^{\intercal}-\overline{L_e})\bar{\Phi}^{-1^{\intercal}}, \tag{23}$$

which, together with equations (21)-(22), allow for the following decomposition of the objective function $\mathscr{J}=\mathscr{I}/T$ in $\widetilde{(P_{\text{e}})}$:

$$\begin{aligned}\mathscr{J}(\bar{Y})&=\mathscr{J}_{\text{QP}}(\bar{Y})+\mathscr{J}_{\mathscr{B}}(\bar{Y}),\\ \mathscr{J}_{\text{QP}}(\bar{Y})&=-\frac{1}{2}\bar{Y}\bar{\Phi}^{-1}\bar{Y}^{\intercal}+\frac{1}{2}\bar{Y}\overline{L_e},\\ \mathscr{J}_{\mathscr{B}}(\bar{Y})&=-\frac{1}{2}\bar{Y}\bar{\Phi}^{-1}\bar{\Phi}_{\Omega}\text{vec}(G(\bar{Y}))+\mathscr{I}_{\text{e}}(\bar{Y}).\end{aligned} \tag{24}$$

Note that the term $\mathscr{I}_{\text{e}}$, defined in (21), can be written in terms of $\bar{Y}$ by virtue of the identity presented in (23). Finally, using the derivation in (24), the moment-based NP $\widetilde{(P_{\text{e}})}$ can be equivalently written as

$$\begin{aligned}\widetilde{(P_{\text{e}})}:\quad \overline{Y^{\text{opt}}}&=\arg\max_{\bar{Y}^{\intercal}\in\mathbb{R}^{\nu}}\mathscr{J}_{\text{QP}}(\bar{Y})+\mathscr{J}_{\mathscr{B}}(\bar{Y}),\\ &\text{subject to}\\ &\bar{Y}\xi\in\mathscr{E},\forall t\in\mathscr{T}_N.\end{aligned} \tag{25}$$

where the corresponding optimal control input is

$$u_N^{\text{opt}}=\left(-(\overline{Y^{\text{opt}}}+\text{vec}(G(\overline{Y^{\text{opt}}}))^{\intercal}\bar{\Phi}_{\Omega}^{\intercal}-\overline{L_e})\bar{\Phi}^{-1^{\intercal}}\right)\xi. \tag{26}$$

Note that (25) is carried over $\bar{Y}$ *only*, and the moment-based equality constraint in (20) has been effectively included as part of the control objective function by virtue of (24). The set $\mathscr{E}$ in (25) denotes an "extended" set of constraints for $\bar{Y}$, which now also includes any control-related limitations, written as a function of $\bar{Y}$ via (23).

As in the ideal PTO OCP case, discussed in [10], the resulting moment-based NP in (25) is constructed as the sum of a quadratic function $\mathscr{J}_{\text{QP}}$, and a 'perturbation' term $\mathscr{J}_{\mathscr{B}}$, which explicitly depends both on the nonlinear mapping g in (5), and

the non-ideal electrical conversion component of the control objective $\mathscr{I}_{\mathrm{e}}$. Furthermore, the quadratic term $\mathscr{J}_{\mathrm{QP}}$, characterised by the Hessian matrix $\mathscr{H} = \bar{\Phi}^{-1} + \bar{\Phi}^{-1^{\mathsf{T}}}$, coincides with that derived in [31], and is always strictly concave, *i.e.* $\lambda(\mathscr{H}) \subset \mathbb{R}^{-}/0$. Since, in addition, for any admissible $\bar{Y}$, the maps $\bar{Y} \mapsto G(\bar{Y})$ and $\bar{Y} \mapsto \mathscr{I}_{\mathrm{e}}(\bar{Y})$ are smooth and bounded, the NP defined in $\widetilde{(P_{\mathrm{e}})}$ always admits a globally optimal solution, *i.e.* it is well-posed. This, naturally, allows for the utilisation of efficient numerical optimisation routines to compute a solution for the moment-based energy-maximising optimal control law under non-ideal PTO behaviour. Note that boundness of the map $\bar{Y} \mapsto \mathscr{J}_{\mathscr{B}}(\bar{Y})$ is necessary and sufficient to guarantee existence of a global energy-maximising solution for (25) (see *e.g.* [32–34]), *i.e.* no assumption is made on the norm of the associated bound. We do note, although, that the 'size' of such a perturbation term, measured in terms of a suitable norm, plays a role on the definition of the associated search space, considered for solving (25) in practice. We refer the reader to [10, Section 5] for further detail.

5 Numerical results

We present, in this section, a numerical appraisal of the moment-based control technique discussed in Section 4, for the point absorber WEC system described in Section 2, considering a non-ideal PTO energy conversion stage. The (linear) hydrodynamic coefficients characterising system Σ in equation (5) are computed via so-called boundary element methods (BEMs). In particular, we consider the open-source hydrodynamic BEM solver NEMOH (see [35]). The set of coefficients $\{\alpha_v, \beta_{r_0}, \beta_{r_1}, \beta_{r_2}\} \subset \mathbb{R}$, which characterise the nonlinear mappings f_v and f_{re}, respectively, are adopted from [10]. For the sake of completeness, Figure 3 provides a graphical description of both linear and nonlinear dynamic contributions associated with system Σ. In particular, Figure 3 (left) illustrates the Bode plot associated with the linear input-output behaviour of equation (5), while Figure 3 (right) shows the 'magnitude' of the associated nonlinear effects (measured in terms of the 2-norm $\|g(x)\|$), as a function of the first two state variables $x_1 = z$ (device displacement) and $x_2 = \dot{z}$ (device velocity). Note that, as soon as the device moves away from the physical equilibrium position $(x_1, x_2) = (0,0)$, $\|g(x)\|$ grows rapidly, stressing the relevance of the nonlinear effects as soon as the WEC departs from 'small motion' conditions.

For the evaluation of the control performance, we consider a randomly generated irregular excitation input, whose stochastic characterisation corresponds with a JONSWAP spectrum [36] with a significant wave height $H_s = 2$ [m], peak enhancement factor $\gamma = 3.3$, and typical peak period of $T_p = 8$ [s]. Note that the latter is chosen relatively far from the resonance period of the point absorber (see the Bode plot in Figure 3), so as to fully demonstrate the capabilities of the controller to maximise energy when the exciting sea-state is far from being 'naturally resonant'

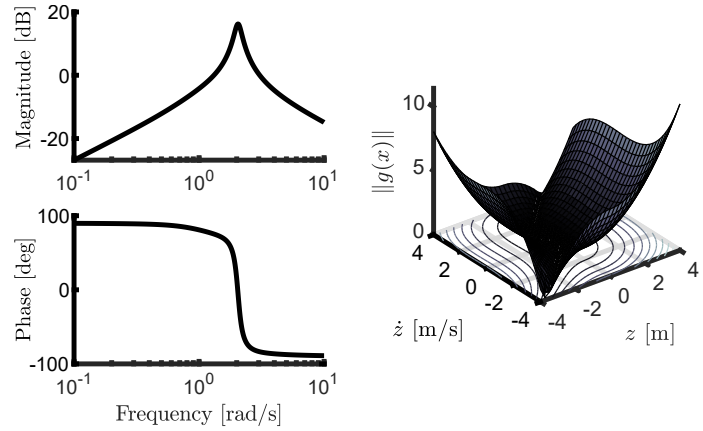

FIGURE 3. Graphical account of both linear and nonlinear dynamic contributions associated with system Σ, for the point absorber WEC under scrutiny.

with the device dynamics.

Regarding the specific parameters characterising the receding-horizon control calculation defined in (25), we set the length of the receding time-window to $T = 10$ [s], which provides an accurate, yet computationally efficient (*i.e.* real-time compatible), representation of both controllable and uncontrollable inputs, without significantly compromising optimality[8]. The corresponding receding time-step is set to $\Delta_h = 0.1$ [s], which is one order of magnitude lower than the typical sampling time for a full-scale device (see *e.g.* [10]). The value ν in (15) is set to $\nu = 16$, which corresponds with a maximum k of $k_{max} = 8$, and hence problem $\widetilde{(P_e)}$ is carried over $\mathbb{R}^{16}$. The set of state and input constraints $\mathscr{E}$ is defined such that $|z| < 2$ [m], $|\dot{z}| < 2$ [m/s], and $|u_N| < 1 \times 10^6$ [N]. Finally, the approximation parameter l, used to define the approximate efficiency map in (19), is set to $l = 1$. The algorithm used to solve the NP $\widetilde{(P_{\mathrm{e}})}$ is based upon the interior-point method described in [37], implemented in MATLAB SIMULINK®.

Figure 5 shows normalised cumulative electrical energy absorption for different values of the efficiency factor μ in the set $[0.7, 1]$. Note that the normalisation is performed against the maximum energy capture value, naturally achieved for the ideal PTO efficiency case, *i.e.* with $\mu = 1$. Consistent with the different 'levels' of losses, defined by μ, the electrical energy absorbed by the device under controlled conditions progressively drops for lower efficiency values, as expected.

To further analyse the effect of different PTO efficiencies on the nature of the computed optimal control solution, Figure 4 shows instantaneous electrical power (top), and moment-based

[8]The larger the value of T, the closer the computed control solution is to the optimal steady-state energy-maximising motion, though also naturally implying a higher computational demand (see [13] for a thorough discussion on this trade-off)

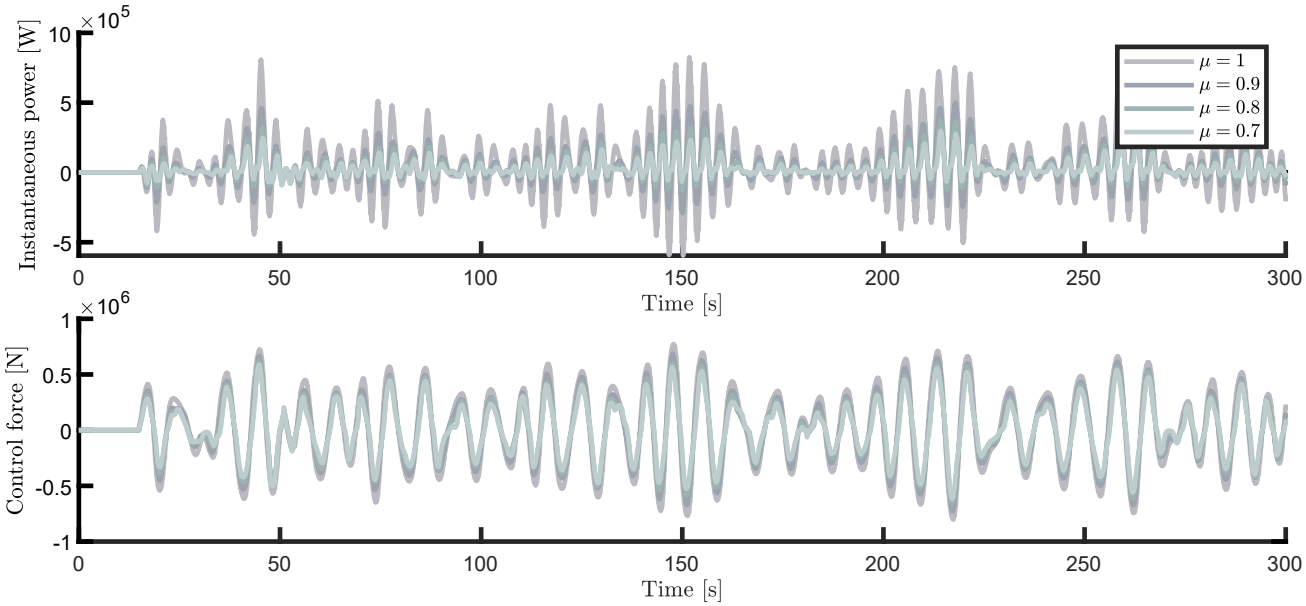

FIGURE 4. Instantaneous power (top), and moment-based optimal control force (bottom), for different efficiency factors $\mu \in [0.7, 1]$.

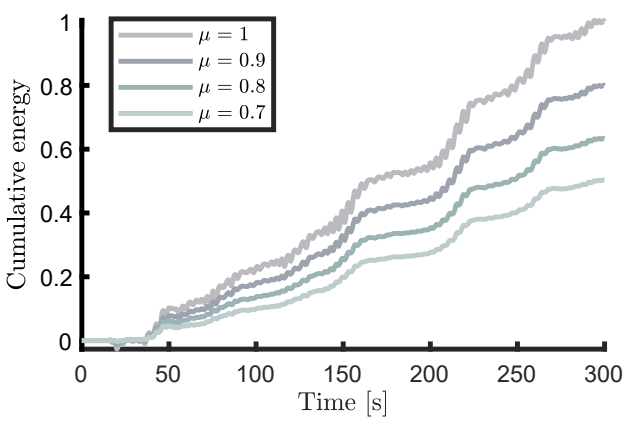

FIGURE 5. Normalised cumulative energy absorption for different values of efficiency factor μ.

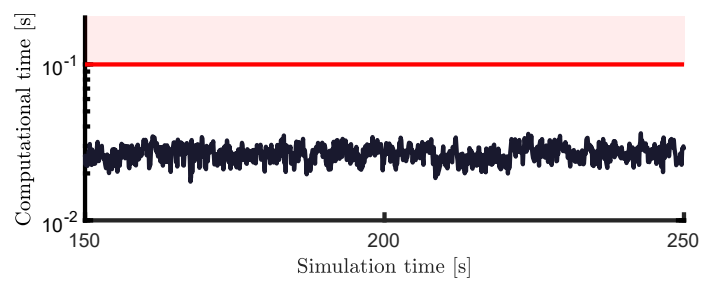

FIGURE 6. Computational time (in [s]) required by each corresponding control calculation as a function of the simulation time (in [s]). The horizontal red line indicates the real-time limit, defined by Δ_h.

optimal control force (bottom), for $\mu \in [0.7, 1]$. Note that, for the ideal PTO case ($\mu = 1$), the control solution demands a relatively large amount of reactive power flow, which is inherently required to effectively enforce resonance of the device with the incoming wave field. This, naturally, leads to higher values of energy absorption in such idealised PTO conversion conditions. As μ decreases, the efficiency of the PTO progressively deteriorates, especially for the reactive power flow condition. Being aware of such non-ideal conversion behaviour, the control solution avoids an excessive requirement of power injection to the WEC, being increasingly 'more passive' as the value of μ decreases.

Figure 6 presents a numerical appraisal of the real-time capabilities of the presented control strategy, explicitly showing computational time (in [s]) required to compute[9] the associated control input for $\mu = 0.8$, as a function of the simulation time (in [s]). Note that all controller computations are performed with a computational requirement significantly lower than the limit $\Delta_h = 0.1$ [s], *i.e.* it achieves real-time consistently.

Finally, and to provide a benchmark comparison case with standard well-established WEC control techniques, Figure 7 shows normalised electric energy absorption for the proposed moment-based controller, and that for a proportional-integral (PI) control structure, designed to interpolate the so-called optimal impedance-matching frequency response mapping[10] at the

[9] On a laptop featuring an Intel® Processor i7-11800H and 16Gb RAM.

[10] The corresponding impedance-matching condition is computed via the linearisation of system Σ in (5) about the equilibrium position. The reader is referred to [6] for a thorough discussion on this topic.

peak frequency characterising the wave excitation input, *i.e.* $\omega_I = 2\pi/T_p = 2\pi/8$ [rad/s]. The normalisation in Figure 7 is performed in terms of the maximum electrical energy absorption value, which corresponds to the moment-based control solution under ideal PTO efficiency conditions. Note that, not only is the PI controller always suboptimal with respect to the proposed solution, but it can effectively produce *negative electrical power absorption*, even for a relatively mild drop in efficiency. On the contrary, being aware of the non-ideal conversion behaviour of the associated PTO, the proposed moment-based control solution is able to consistently maximise absorption, always producing a positive energy balance.

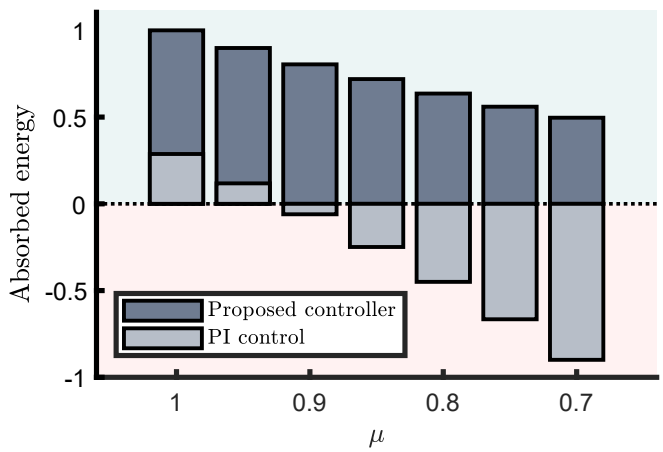

FIGURE 7. Normalised electrical energy absorption for the proposed moment-based solution, and a benchmark PI controller.

6 Conclusions

We present, in this paper, a nonlinear moment-based energy-maximising control solution for WEC systems under non-ideal PTO behaviour. We show that the mathematical formalism which underlies moment-based theory can be effectively used to transcribe the corresponding infinite-dimensional OCP, characterising non-ideal electrical energy absorption, to a finite-dimensional (tractable) NP. We further show the resulting NP is well-posed, *i.e.* it always admits a globally optimal energy-maximising solution, facilitating the application of state-of-the-art numerical routines, leading to real-time capabilities. Numerical results are presented for a particular heaving point absorber WEC system, explicitly illustrating the capabilities of the proposed controller to maximise energy extraction in a non-ideal PTO conversion scenario, including a comparison against a benchmark PI control strategy, showing that the proposed nonlinear controller outperforms such a benchmark case for every considered PTO operating scenario.

ACKNOWLEDGMENT

This project has received funding from the European Union's Horizon 2020 research and innovation programme under the Marie Sklodowska-Curie grant agreement No 101024372. The results of this publication reflect only the author's view and the European Commission is not responsible for any use that may be made of the information it contains

REFERENCES

[1] Ringwood, J., Bacelli, G., and Fusco, F., 2014. "Energy-maximizing control of wave-energy converters: The development of control system technology to optimize their operation". *IEEE Control Systems,* ***34***(5), pp. 30–55.

[2] Korde, U. A., and Ringwood, J. V., 2016. *Hydrodynamic control of wave energy devices*. Cambridge University Press.

[3] Faedo, N., Olaya, S., and Ringwood, J. V., 2017. "Optimal control, MPC and MPC-like algorithms for wave energy systems: An overview". *IFAC Journal of Systems and Control,* ***1***, pp. 37–56.

[4] Ringwood, J. V., 2020. "Wave energy control: status and perspectives 2020". *IFAC-PapersOnLine,* ***53***(2), pp. 12271–12282.

[5] Ringwood, J. V., Mérigaud, A., Faedo, N., and Fusco, F., 2019. "An analytical and numerical sensitivity and robustness analysis of wave energy control systems". *IEEE Transactions on Control Systems Technology,* ***28***(4), pp. 1337–1348.

[6] Faedo, N., Carapellese, F., Pasta, E., and Mattiazzo, G., 2022. "On the principle of impedance-matching for underactuated wave energy harvesting systems". *Applied Ocean Research,* ***118***, p. 102958.

[7] Genest, R., Bonnefoy, F., Clément, A. H., and Babarit, A., 2014. "Effect of non-ideal power take-off on the energy absorption of a reactively controlled one degree of freedom wave energy converter". *Applied Ocean Research,* ***48***, pp. 236–243.

[8] Bacelli, G., Genest, R., and Ringwood, J. V., 2015. "Nonlinear control of flap-type wave energy converter with a non-ideal power take-off system". *Annual Reviews in Control,* ***40***, pp. 116–126.

[9] Mérigaud, A., and Tona, P., 2020. "Spectral control of wave energy converters with non-ideal power take-off systems". *Journal of Marine Science and Engineering,* ***8***(11), p. 851.

[10] Faedo, N., Scarciotti, G., Astolfi, A., and Ringwood, J. V., 2021. "Nonlinear energy-maximizing optimal control of wave energy systems: A moment-based approach". *IEEE Transactions on Control Systems Technology,* ***29(6)***, pp. 2533–2547.

[11] Faedo, N., Scarciotti, G., Astolfi, A., and Ringwood, J. V., 2021. "Energy-maximising moment-based constrained op-

timal control of ocean wave energy farms". *IET Renewable Power Generation,* ***15***(14), pp. 3395–3408.

[12] Faedo, N., 2020. "Optimal control and model reduction for wave energy systems: A moment-based approach". PhD thesis, Department of Electronic Engineering, Maynooth University.

[13] Faedo, N., Peña-Sanchez, Y., and Ringwood, J. V., 2020. "Receding-horizon energy-maximising optimal control of wave energy systems based on moments". *IEEE Transactions on Sustainable Energy,* ***12***(1), pp. 378–386.

[14] Astolfi, A., 2010. "Model reduction by moment matching for linear and nonlinear systems". *IEEE Transactions on Automatic Control,* ***55***(10), pp. 2321–2336.

[15] Astolfi, A., Scarciotti, G., Simard, J., Faedo, N., and Ringwood, J. V., 2020. "Model reduction by moment matching: Beyond linearity a review of the last 10 years". In 59th IEEE Conference on Decision and Control (CDC), IEEE, pp. 1–16.

[16] Hals, J., Ásgeirsson, G. S., Hjálmarsson, E., Maillet, J., Möller, P., Pires, P., Guérinel, M., and Lopes, M., 2016. "Tank testing of an inherently phase-controlled wave energy converter". *International Journal of Marine Energy,* ***15***, pp. 68–84.

[17] Faedo, N., Piuma, F. J. D., Giorgi, G., and Ringwood, J. V., 2020. "Nonlinear model reduction for wave energy systems: a moment-matching-based approach". *Nonlinear Dynamics,* ***102***(3), pp. 1215–1237.

[18] Falnes, J., and Kurniawan, A., 2020. *Ocean Waves And Oscillating Systems: Linear Interactions Including Wave-Energy Extraction*, Vol. 8. Cambridge University Press.

[19] Faedo, N., Peña-Sanchez, Y., and Ringwood, J. V., 2020. "Parametric representation of arrays of wave energy converters for motion simulation and unknown input estimation: a moment-based approach". *Applied Ocean Research,* ***98***, p. 102055.

[20] Pérez, T., and Fossen, T. I., 2008. "Time-vs. frequency-domain identification of parametric radiation force models for marine structures at zero speed". *Modeling, Identification and Control,* ***29***(1), pp. 1–19.

[21] Morison, J., Johnson, J., Schaaf, S., et al., 1950. "The force exerted by surface waves on piles". *Journal of Petroleum Technology,* ***2***(05), pp. 149–154.

[22] Liberzon, D., 2011. *Calculus of variations and optimal control theory*. Princeton university press.

[23] Mattingley, J., Wang, Y., and Boyd, S., 2011. "Receding horizon control". *IEEE Control Systems Magazine,* ***31***(3), pp. 52–65.

[24] Tona, P., Nguyen, H.-N., Sabiron, G., and Creff, Y., 2015. "An efficiency-aware model predictive control strategy for a heaving buoy wave energy converter". In 11th European Wave and Tidal Energy Conference (EWTEC).

[25] Ringwood, J., Ferri, F., Tom, N., Ruehl, K., Faedo, N., Bacelli, G., Yu, Y.-H., and Coe, R. G., 2019. "The wave energy converter control competition: Overview". In International Conference on Offshore Mechanics and Arctic Engineering, Vol. 58899, American Society of Mechanical Engineers, p. V010T09A035.

[26] Mérigaud, A., Ngo, C., Nguyen, H.-N., Sabiron, G., and Tona, P., 2020. "Ex-post analysis of the wec control competition results using a fourier spectral control approach". *IFAC-PapersOnLine,* ***53***(2), pp. 12319–12326.

[27] Von Stryk, O., 1993. "Numerical solution of optimal control problems by direct collocation". In *Optimal control*. Springer, pp. 129–143.

[28] Isidori, A., 2013. *Nonlinear control systems*. Springer Science & Business Media.

[29] Faedo, N., Scarciotti, G., Astolfi, A., and Ringwood, J. V., 2021. "On the approximation of moments for nonlinear systems". *IEEE Transactions on Automatic Control,* ***66(11)***, pp. 5538–5545.

[30] Urabe, M., 1965. "Galerkin's procedure for nonlinear periodic systems". *Archive for Rational Mechanics and Analysis,* ***20***(2), pp. 120–152.

[31] Faedo, N., Scarciotti, G., Astolfi, A., and Ringwood, J. V., 2018. "Energy-maximising control of wave energy converters using a moment-domain representation". *Control Engineering Practice,* ***81***, pp. 85–96.

[32] Phu, H. X., Pho, V., and An, P., 2011. "Maximizing strictly convex quadratic functions with bounded perturbations". *Journal of Optimization Theory and Applications,* ***149***(1), pp. 1–25.

[33] Phu, H., and Pho, V., 2012. "Some properties of boundedly perturbed strictly convex quadratic functions". *Optimization,* ***61***(1), pp. 67–88.

[34] Phu, H. X., 2008. "Outer γ-convexity in vector spaces". *Numerical Functional Analysis and Optimization,* ***29***(7-8), pp. 835–854.

[35] Babarit, A., and Delhommeau, G., 2015. "Theoretical and numerical aspects of the open source BEM solver NEMOH". In 11th European Wave and Tidal Energy Conference, Nantes.

[36] Hasselmann, K. F., Barnett, T. P., Bouws, E., Carlson, H., Cartwright, D. E., Eake, K., Euring, J., Gicnapp, A., Hasselmann, D., Kruseman, P., et al., 1973. "Measurements of wind-wave growth and swell decay during the joint north sea wave project (JONSWAP).". *Ergaenzungsheft zur Deutschen Hydrographischen Zeitschrift, Reihe A*.

[37] Waltz, R. A., Morales, J. L., Nocedal, J., and Orban, D., 2006. "An interior algorithm for nonlinear optimization that combines line search and trust region steps". *Mathematical programming,* ***107***(3), pp. 391–408.